



**HAL**  
open science

## Photosensitivity of Infrared Glasses under Femtosecond Laser Direct Writing for mid-IR Applications

Pierre Delullier, Laurent Calvez, Guillaume Druart, Florence de La Barrière, Christophe Humbert, Bertrand Poumellec, Matthieu Lancry

► **To cite this version:**

Pierre Delullier, Laurent Calvez, Guillaume Druart, Florence de La Barrière, Christophe Humbert, et al.. Photosensitivity of Infrared Glasses under Femtosecond Laser Direct Writing for mid-IR Applications. Applied Sciences, 2022, 12 (17), pp.8813. 10.3390/app12178813 . hal-03771407

**HAL Id: hal-03771407**

**<https://hal.science/hal-03771407v1>**

Submitted on 7 Sep 2022

**HAL** is a multi-disciplinary open access archive for the deposit and dissemination of scientific research documents, whether they are published or not. The documents may come from teaching and research institutions in France or abroad, or from public or private research centers.

L'archive ouverte pluridisciplinaire **HAL**, est destinée au dépôt et à la diffusion de documents scientifiques de niveau recherche, publiés ou non, émanant des établissements d'enseignement et de recherche français ou étrangers, des laboratoires publics ou privés.

Article

# Photosensitivity of Infrared Glasses under Femtosecond Laser Direct Writing for mid-IR Applications

Pierre Delullier <sup>1,2,\*</sup>, Laurent Calvez <sup>3</sup>, Guillaume Druart <sup>1</sup>, Florence De La Barrière <sup>1</sup>, Christophe Humbert <sup>4</sup>, Bertrand Poumellec <sup>2</sup> and Matthieu Lancry <sup>2</sup>

<sup>1</sup> ONERA, The French Aerospace Lab, 91120 Palaiseau, France

<sup>2</sup> ICMMO, Institut de Chimie Moléculaire et des Matériaux d'Orsay, Université Paris-Saclay, 91405 Orsay, France

<sup>3</sup> Institut des Sciences Chimiques de Rennes, Université Rennes, UMR6226, 35000 Rennes, France

<sup>4</sup> Institut de Chimie Physique, Université Paris-Saclay, CNRS, UMR8000, 91405 Orsay, France

\* Correspondence: pierre.delullier@onera.fr

**Abstract:** Chalcogenide glasses are increasingly being developed for photonic applications, particularly in the field of mid-infrared optical imaging. In this paper, we study the photosensitivity of one chalcogenide to direct femtosecond laser writing and its possible applications to micro-optics. Particular attention has been paid to the creation of phase changes and related refractive index variations. This chalcogenide glass was compared with two commercial heavy oxide glasses: Schott SF10 and Corning 9754. We observed different types of permanent modifications depending on the writing speed and the laser pulse energy. Index variations were measured at  $\Delta n > +0.055$  in the chalcogenide glass while maintaining spectral transmission similar to the pristine materials before irradiation. This provides a good candidate to design optical components for infrared application and helps to unlock the potential of the femtosecond laser direct writing technique to implement at high writing speed and high index changes with low optical losses.

**Keywords:** optical glasses; chalcogenide; optical components; femtosecond laser writing; IR optics

**Citation:** Delullier, P.; Calvez, L.; Druart, G.; De La Barrière, F.; Humbert, C.; Poumellec, B.; Lancry, M. Photosensitivity of Infrared Glasses under Femtosecond Laser Direct Writing for mid-IR Applications. *Appl. Sci.* **2022**, *12*, 8813. <https://doi.org/10.3390/app12178813>

Academic Editor: Maria Amélia Ramos Loja

Received: 9 August 2022

Accepted: 30 August 2022

Published: 1 September 2022

**Publisher's Note:** MDPI stays neutral with regard to jurisdictional claims in published maps and institutional affiliations.



**Copyright:** © 2022 by the authors. Licensee MDPI, Basel, Switzerland. This article is an open access article distributed under the terms and conditions of the Creative Commons Attribution (CC BY) license (<https://creativecommons.org/licenses/by/4.0/>).

## 1. Introduction

Direct laser writing consists in focusing a high-intensity laser inside a crystalline or an amorphous material in order to locally modify its physical properties [1]. Since their development about thirty years ago, femtosecond lasers have been used in particular for this laser writing technique. Thanks to ultra-short pulses, these lasers can reach intensities higher than  $\text{TW}/\text{cm}^2$  at the focal point. With non-linear absorption of the material due to these high intensities, the material is permanently modified in a confined volume of a few  $\mu\text{m}^3$ . This direct femtosecond laser writing (FLDW) is therefore of great interest for its numerous writing possibilities, as well as for a number of accessible materials, especially in the fabrication of complex 3D photonic components. Indeed, current advanced femtosecond laser systems offer a myriad of material interactions in glassy media: nanocrystals precipitation [2], metallic nanoparticles precipitation and shaping [3], nanogratings formation [4], or 3D refractive index changes profiling (based on nanoscale structural changes) [1]. These materials' interactions depend on both the laser parameters and the material chemical composition. The FLDW technique is especially studied for the creation of nanogratings and optical waveguides [5] but attracts the attention of researchers in many different fields such as diffractive and polarization optics but also gradient index optics [6] and geometric phase optics [7].

This technique has been extensively studied in silica in order to fabricate new integrated optical components: waveguides, lenses, birefringent optics, etc. However, these studies are mainly limited to visible and near-infrared wavelengths [1,8,9]. Today,

the studies of the FLDW technique are growing in materials such as silicon performing in infrared [10]. Indeed, the development of integrated optical components in infrared has many attractive civilian (home automation, smartphones, automotive, etc.) and military applications.

The materials that can be used at mid-wavelength infrared (MWIR: 3–5  $\mu\text{m}$ ) and long-wavelength infrared (LWIR: 8–12  $\mu\text{m}$ ), besides silicon, are non-silicate glasses such as chalcogenides [11], fluorides [12], and heavy oxide glasses [13]. In particular, chalcogenide materials have a very wide transmission band from visible to LWIR (8–14  $\mu\text{m}$ ). Despite their growing use in the field of infrared optical imaging for their optical qualities, studies of their utilization with fs-laser writing are mainly limited to the fabrication of mid-IR waveguides for space applications [5,12]. The use of the FLDW technique to fabricate complex optical components embedded in these infrared materials is a fairly new and developing area [5,14].

In order to open the door to the fast prototyping of complex 3D optics (geometric phase lens, gradient index optics, etc.) for infrared applications, our study seeks to understand the modifications implemented in a set of well-chosen glasses as a function of the writing parameters (laser pulse duration, pulse energy, writing speed, etc.). We are particularly interested in the quantification of both phase and refractive index modifications, which would allow the 3D inscription of freeform objects that are more and more developed in optical imaging [15]. According to the literature, chalcogenide glasses can reach very high index contrasts: higher than  $\sim 5 \times 10^{-2}$  [16], while heavy oxides reach lower values of a few  $10^{-3}$  [13], but they have better thermal and mechanical stability. Besides chalcogenides, heavy oxide glasses transmit only up to MWIR, but they are chemically stable, manufacturable by conventional means (melt-quenching), and mechanically resistant. In this paper, we study the photosensitivity of one chalcogenide glass: 75(GeS<sub>2</sub>)-15(In<sub>2</sub>S<sub>3</sub>)-10(CsCl), also named GeS<sub>2</sub>. Two commercial heavy oxide glasses are also studied: Schott SF10 (a lead oxide silicate) and Corning 9754 (a calcium aluminogermanate glass), named, respectively, SF10 and 9754 in the following. Here, we compare the main optical performances under FLDW: types of modifications, thresholds of appearance according to laser energy and writing speed, refractive index variations, and photo-induced spectral losses.

## 2. Materials and Methods

The three glasses studied here are divided into 2 categories. On the one hand, the heavy oxides have a rather low refractive index, and their transmission range does not go further than  $\sim 5 \mu\text{m}$ . On the other hand, the chalcogenide has a refractive index higher than 2 (see Table 1) and its transparency extends up to 11.5  $\mu\text{m}$ . In order to spatially control the laser writing process, the samples (polished on both sides) are placed on a computer-controlled platform with three translation axes. We use the commercial Satsuma laser (Amplitude Systèmes, Pessac, France) whose amplifier is a Yb-doped fiber. In this paper, the following laser parameters are fixed: an 800 fs pulse duration, a 1030 nm central wavelength, and a repetition rate fixed at 100 kHz. An aspherical lens with a 0.6 numerical aperture allows us to focus the laser beam at 500  $\mu\text{m}$  below the substrate surface. The focused beam spot  $\Phi_{\text{laser}}$  can be calculated as follows:

$$\Phi_{\text{laser}} = \frac{\lambda M^2}{\pi NA} \approx 1.2 \mu\text{m} \quad (1)$$

with  $\lambda$  as the central wavelength of the laser,  $M^2 = 1.09$  as the beam quality factor, and  $NA$  as the numerical aperture of our microscope objective.

The scanning speed of the sample (thanks to the scanning platform) and the laser energy are variable. In order to inscribe more complex shapes than simple waveguides and more oriented towards optics or micro-optics, we write discs with a diameter of 100  $\mu\text{m}$ . To write homogeneous discs, the displacement of the sample follows a spiral trajectory with a step of 1  $\mu\text{m}$ . The writing speed varies from 0.01 mm/s to 25 mm/s, which

corresponds to a pulse density ranging from  $1.2 \times 10^4$  pulses/ $\mu\text{m}$  down to 5 pulses/ $\mu\text{m}$ . The laser energy from 0.01  $\mu\text{J}$  to 2  $\mu\text{J}$  and the polarization was kept linear and oriented along X-axis (that is define by the laser compressor plane).

**Table 1.** Label and refractive index of the samples. The data for the 9754 and the SF10 come from the Corning and Schott datasheets, respectively. For GeS<sub>2</sub> data were measured using refractometry in total internal reflection mode.

Label	$n_{1.55\mu\text{m}}$	$n_{4\mu\text{m}}$
GeS <sub>2</sub> based glass	2.082	2.028
Corning 9754	1.643	1.607
Schott SF10	1.693	1.637

### 3. Results and Discussion

**Determination of the optical modifications landscape in the energy–speed domain:** During laser direct writing, the non-linear absorption of laser energy by the material locally modifies its physical properties. Different types of permanent modifications can then appear according to the defined parameters. Three main types of modifications are defined in the literature [1,10,17]. Type I is defined as the appearance of a smooth, homogeneous, and permanent variation in the refractive index. The threshold for the appearance of the Type I change is at low energy. This type of modification allows 3D engineering of the index profiles with fine control of the refractive index variation. It is therefore a type of modification particularly interesting for the manufacture of optical components, especially in the field of imaging or for optical waveguides and gratings. Type II corresponds to an anisotropic modification of the refractive index whose orientation can be controlled by the writing laser polarization. In most oxide glasses, and according to specific conditions of pulse duration, repetition rate, pulse number and pulse energy, and self-assembled periodic nanostructures can appear and make the glass locally birefringent. With higher laser intensities, voids resulting from micro-explosions can appear in the material: this is the Type III modification. We can finally define the last type of modification appearing at high laser intensities. Often abusively called “heat accumulation regime” in the literature, this modification corresponds to a smooth and homogeneous variation of the refractive index with a significant increase in the size of the modified area compared to the size of the energy source. This spatially broadened Type I modification will therefore be referred to as the “spatial broadening regime” that described this phenomenon more accurately [18].

After the 2D micro-writing of the samples, we made an initial observation with an Olympus BX51 polarized optical microscope in order to determine the thresholds of appearance of the different types of modification. In the following, Type I is defined as a permanent refractive index contrast seen in natural light but not in crossed polarizers and whose size remains limited to the laser beam waist. In contrast, the spatial broadening regime is not necessarily a new type of modification because it is also detected as an isotropic refractive index contrast observed through optical microscopy (so in that sense it is quite similar to Type I). However, its threshold was defined here by an increase of 20% in the imprinted laser track width beyond the beam waist. Type II is detected under polarized optical microscopy and is characterized by the formation of a linear birefringence whose orientation is almost linearly dependent on the laser polarization.

Figure 1 shows the different types obtained as a function of the scanning speed and the laser pulse energy in 9754 and GeS<sub>2</sub> glasses. SF10 has writing-type threshold graphs similar to those of 9754 in Figure 1. In particular, the energy thresholds needed for the appearance of Type I or spatial broadening regimes are similar: about 0.1  $\mu\text{J}$  for Type I and between 1.5  $\mu\text{J}$  and 2  $\mu\text{J}$  for the “spatial broadening regime”. It should be noted, however, that 9754 is the only one, which shows the appearance of Type II, and none of the three materials showed Type III—voids formation. For a low writing speed (typ. 0.01

mm/s) self-assembled periodic nanostructures appear in 9754 glass, creating a birefringence whose neutral axes are oriented by the femtosecond laser polarization [19]. In contrast, we note that the chalcogenide glass has low Type I thresholds of a few nJ at low scanning speeds and a few 10 s nJ at high scanning speeds (> 1 mm/s, up to 25 mm/s). The spatial broadening regime also appears for low energies of a few  $10^{-1}$   $\mu$ J. On the contrary, SF10 and 9754 oxide glasses show thresholds of about one order higher for both Type I threshold and spatial broadening regime. Taking into account the size of the laser beam, we can express the Type I thresholds in terms of fluence ( $\text{J}/\text{cm}^2$ ). In our typical writing conditions, at the scanning speed of 1 mm/s, we calculate the corresponding fluence per pulse in  $\text{GeS}_2$  at  $2.7 \text{ J}/\text{cm}^2$ , in 9754 at  $11.1 \text{ J}/\text{cm}^2$ , and in SF10 at  $13.3 \text{ J}/\text{cm}^2$ .

Moreover, the threshold of appearance of the different regimes depends on the number of pulses sometimes called the “incubation effect”. Typically, one can find a decrease by a factor of 2 for oxide glasses, e.g., from  $13.3 \text{ J}/\text{cm}^2$  to  $6.6 \text{ J}/\text{cm}^2$  in SF10 when decreasing the speed down to 0.01 mm/s (i.e.,  $1.2 \times 10^4$  pulses/ $\mu\text{m}$ ). Following a similar trend in  $\text{GeS}_2$ , but more pronounced, the threshold decreases progressively from  $4.4 \text{ J}/\text{cm}^2$  for 5 pulses/ $\mu\text{m}$  (speed of 25 mm/s) to  $2.7 \text{ J}/\text{cm}^2$  for 120 pulses/ $\mu\text{m}$  and down to  $0.4 \text{ J}/\text{cm}^2$  for  $1.2 \times 10^4$  pulses/ $\mu\text{m}$  (0.01 mm/s). We also note that the size (longitudinal) of the modified zone increases with the energy but not with the number of pulses; on the other hand, the  $\Delta n$  increases with the number of pulses. In addition, the width of the laser tracks remains quite similar within the whole Type I regime. This contrasts with the so-called spatial broadening regime where the width increases progressively with the pulse energy.

Therefore, we suggest here that Type I modifications are related to the accumulation of point defects leading to a glass network depolymerization, which favors a structural relaxation. For example, this is confirmed in  $\text{GeS}_2$  by Raman measurements indicating that the refractive index increase is associated not only to point defects generation but rather to glass densification (e.g., an increase in the population of edge-sharing tetrahedra in  $\text{GeS}_2$ ) [20]. Then, in agreement with the literature, the measured Type I thresholds decrease when the number of pulses increases. Indeed, using moderate focusing (0.25 NA), Schäffer et al. [21] observed “incubation effects” leading to a decrease in the damage threshold in oxide glasses when increasing the number of pulses, as observed during surface experiments [22,23]. In the latter case, it has been demonstrated [24] that the effect of incubation is twofold: (i) it modifies the absorption by the accumulation of point defects, and (ii) it introduces new possibilities of energy deposition in the glass network, e.g., in addition to electron-phonon coupling. These possibilities are based on a coupling of electrons trapped in the lattice. The increase in defect concentration is proportional to the initial defect concentration and the increment in the number of pulses and also depends on the number of atomic sites likely to be affected during this accumulation process.

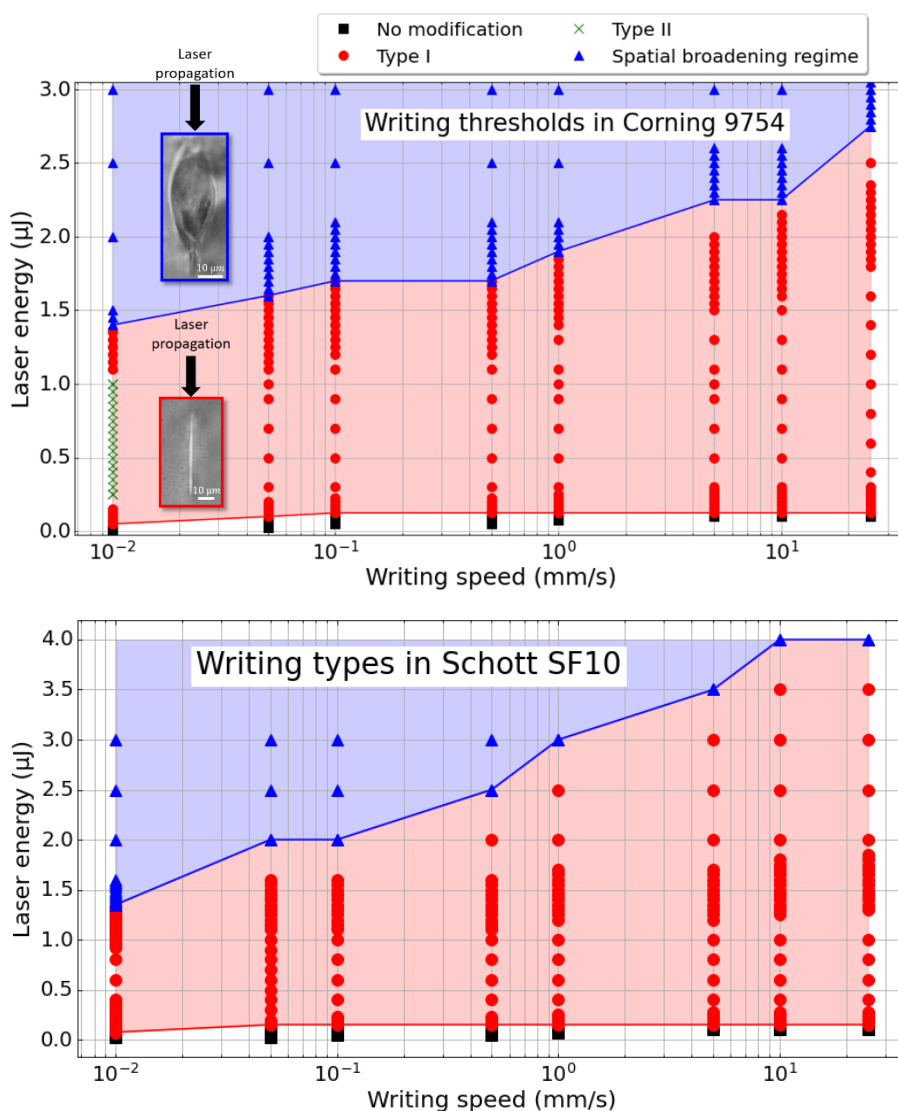
Then, there is likely a second mechanism acting in the spatial broadening regime, which enlarges progressively the laser track’s width. In a simplified view, the spatial extension of the laser tracks (beyond the light beam size) is likely related to a temperature increase with the pulse energy [25]. Now, if we increase the energy of the pulses, the maximum temperature reached at the laser focal point increases but the spatial distribution of heat (defined by the Fourier’s law) remains unchanged. The maximum temperature is given by [25]:

$$T_{\max} = \frac{AE_p}{\pi^{3/2}\rho C_p w_0^2 w_z} \quad (2)$$

where  $AE_p$  is the energy absorbed per unit volume,  $\rho$  is the glass density,  $C_p$  is the heat capacity,  $w_0$  is the beam waist radius, and  $w_z$  is the longitudinal laser beam size (depending on the NA, pulse duration, and non-linear effects). Thus, the increase in energy  $E_p$  induces an increase in temperature  $T_{\max}$  and thus a spatial enlargement (beyond the light affected zone) of the imprinted laser track. This corresponds to the

volume within which the temperature is higher than a threshold temperature (i.e., a transformation temperature), leading to glass structural relaxation and thus permanent index changes.

From that point, one could explain the decrease in the spatial broadening threshold when the writing speed decrease, which is a general trend observed in all three samples. Here, one explanation could be based on the accumulation of point defects (also called color centers) from pulse to pulse. This results in an increase in the absorption coefficient  $A$ , with  $A = \sigma_k \cdot I^k$ , either through an increase in the multiphoton absorption cross-section  $\sigma_k$  or even a reduction in the multiphoton process order  $k$  by passing through a relay state (i.e., an electronic absorption level attributed to a point defect). Then, the resulting increase in energy absorbed per unit of volume ( $AE_p$ ) leads to a reduction in the spatial broadening threshold when reducing the writing speed.



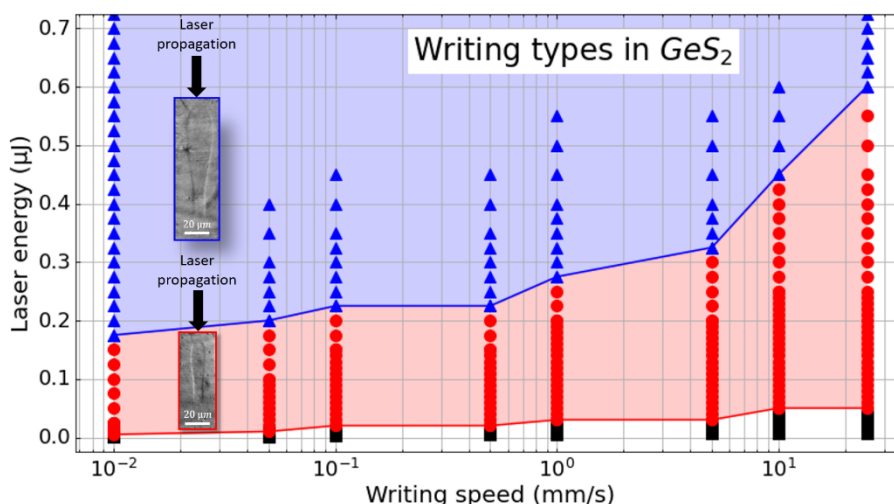


**Figure 1.** On the top, processing windows in the Corning 9754. In the middle, processing windows in the Schott SF10. On the bottom, processing windows in the GeS<sub>2</sub> glass. In the blue areas, images of a spatial broadening regime profiles (criterion: a 20% increase in laser track width compared to the beam waist). In the red areas, images of Type I profiles. Laser parameters: 1030 nm, 800 fs, 100 kHz, 0.6 NA, and linear polarization along X.

**Quantification of the photo-induced refractive index changes:** In addition to microscopic observations, we performed a quantitative measurement of the phase variation implemented by fs-laser direct writing [26]. Using Quantitative Phase Microscopy (QPM, Iatia), we were able to measure a mapping of the localized phase (expressed in rad) compared to the pristine background. To study the photo-induced phase variations, a constant writing speed was set at 1 mm/s. This speed was chosen as a compromise in order to achieve fast laser writing while maintaining a high and constant index profile all along the spiral trajectory. Figure 2 plots the phase variation implemented in each material as a function of laser pulse energy. We notice that a strong phase variation appears at a very low energy in the GeS<sub>2</sub> (about  $2\pi$  rad at  $0.125 \mu\text{J}$ ). We also note that SF10 remains on a nearly constant phase variation above  $0.7 \mu\text{J}$  ( $\sim 1.9$  rad). On the other hand, the 9754 glass exhibits a monotonous growing over a wide range of energies and allows reaching relatively strong phase variations (around  $4\pi$  rad at  $1.7 \mu\text{J}$ ). All these glasses are of interest for the fabrication of 3D geometric phase optics [7]. Variations of  $\pi$  rad with a precise phase distribution are sufficient to create most of the complex optics.

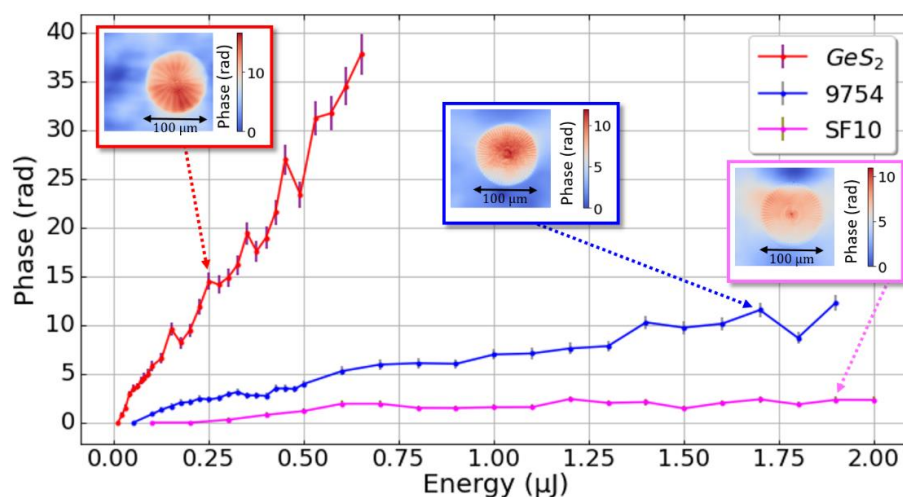


**Figure 2.** Phase variation implemented by the FLDW technique as a function of laser energy. The writing speed of these irradiations is fixed at 1 mm/s (corresponding to about 120 pulses/ $\mu\text{m}$ ). Inset:

an example of a quantitative phase map measured by the Quantitative Phase Microscopy technique has been added for each material. Laser parameters: 1030 nm, 800 fs, 100 kHz, and 0.6 NA.

The FLDW technique locally changes the glass density of the glasses but also creates some point defects, which in turn affect its optical transmission [27]. Therefore, we measured the optical transmission as a function of wavelength for all samples before and after laser irradiation. In order to measure the room temperature's optical transmission of the samples over a wide spectral band, we used two spectrophotometers: an Agilent Cary 5000 ( $\Delta\lambda \in [0.2 ; 3.3] \mu\text{m}$ ) and a Bruker Equinox 55 ( $\Delta\lambda \in [2 ; 20] \mu\text{m}$ ). Thanks to the results presented in Figure 2 of the phase variation as a function of laser energy, we were able to implement a phase change in  $\pi$  rad in our materials. We chose this  $\pi$  rad variation because it is a phase shift particularly used to design Fresnel lenses, binary ring phase masks, etc.

We can observe in Figure 3 a rather important difference in transmission between the chalcogenides, transmitting up to 10–12  $\mu\text{m}$ , and the heavy oxides transmitting only up to 4–5  $\mu\text{m}$ . Then we notice in particular that the difference in transmission before and after femtosecond laser texturing remains quite negligible for a photo-induced phase variation of  $\pi$  rad. Although it is likely that implementing a larger phase variation would imply additional optical losses in these materials, the results in Figure 3 are encouraging and bode well for a small change in the optical transmission of these glasses despite a useful magnitude of the observed changes in the refractive index.

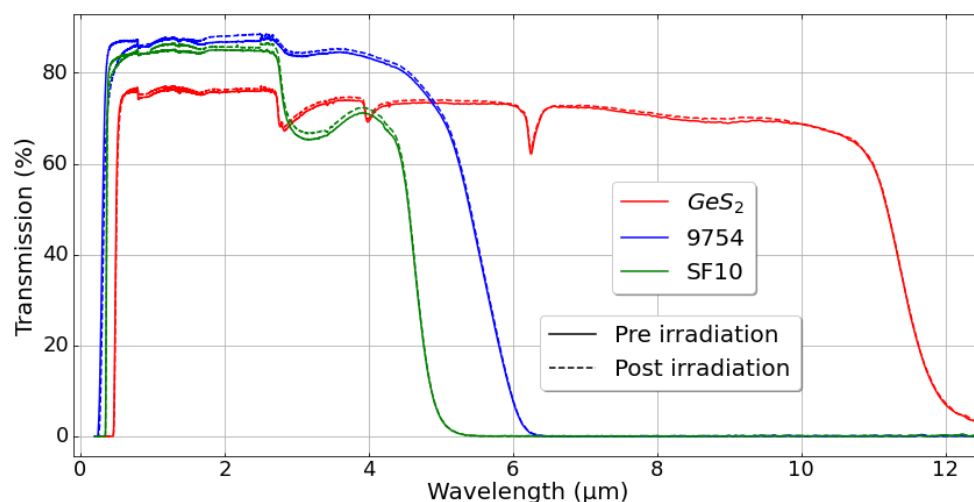


**Figure 3.** Optical transmission of the studied glasses before and after a  $\pi$  rad phase variation was implemented using FLDW. Laser parameters: 1030 nm, 800 fs, 100 kHz, 1 mm/s, 0.6 NA.

We have seen that we are able to implement a strong phase variation in these glasses and more particularly in  $\text{GeS}_2$  because of its binding energy, which is much lower than those of the heavy oxide glasses. The formation energy of  $\text{GeS}_2$  is about  $-0.66$  eV/atom, whereas the formation energy of  $\text{PbO}$  (a key constituent of SF10) is about  $-1.47$  eV/atom and  $-2.07$  eV/atom for  $\text{GeO}_2$  and  $-3.41$  eV/atom for  $\text{Al}_2\text{O}_3$ . These data are extracted from The Material Project website and calculated based on Ref [28]. For many applications, it would be necessary to convert phase variation ( $\varphi$  in rad) into refractive index changes written by the femtosecond laser. In this view, it is sufficient to measure the thickness of the laser-modified region  $d$  to have:

$$\Delta n = \frac{\lambda}{2\pi d} \varphi, \quad (3)$$

where  $\lambda$  is the probe wavelength used for the quantitative phase measurement (here  $\lambda = 550$  nm). This value of  $\Delta n$  is only an approximation. Indeed, it is assumed that the FLDW technique implements a constant index variation over a cylinder in the thickness of the



material. In fact, the real shape of the trace depends first of all on the focusing optics, on the index, and on the non-linear index of the material. There is then a competition between the Kerr effect focusing the rays and the defocusing due to the plasma created by the fs-laser [29].

Nevertheless, we aim to use the FLDW technique to fabricate gradient index optics and geometric phase optics for infrared imaging systems. Thus, for the fabrication of graded index optics, we need to know the index variation implemented by the laser. One of the current development axes of the direct femtosecond laser writing technique is to find the materials and the laser parameters allowing one to obtain the highest possible refractive index variations. Indeed, the greater the range of index variation available, the more freedom the optical designer will have to create the optical component needed for their system. We have therefore reviewed in Figure 4 the different ranges of index variation obtained in the literature (data collected from Refs. [5,9,18,29–31]). Several glass families are considered, in particular mid-IR glasses: fluorides, chalcogenides, and heavy oxides, including Barium Gallo-Germanate (BGG).

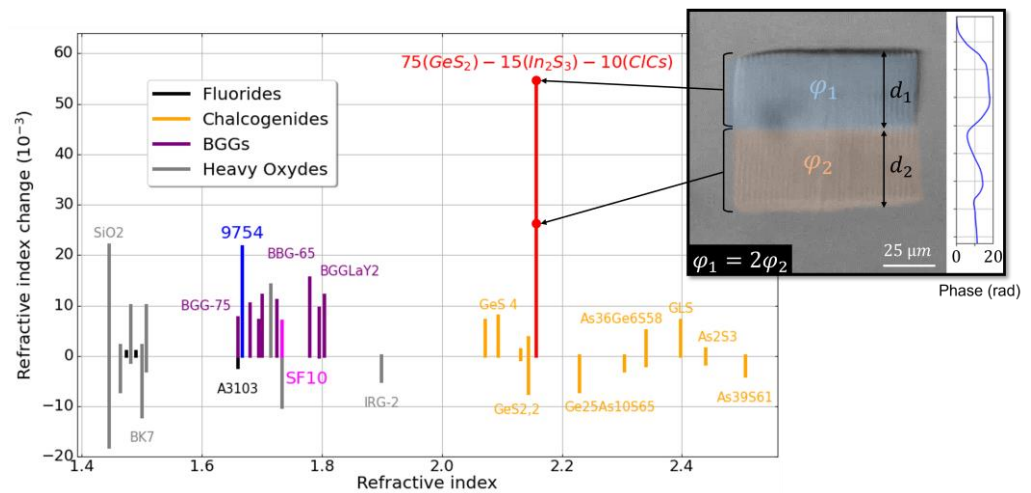


**Figure 4.** Range of refractive index variation induced by fs-laser vs. refractive index (typ. Measured at 550 nm) for different glasses. Our materials: GeS<sub>2</sub> in red, Corning 9754 in blue, and Schott SF10 in pink. Inset: a false color image of a textured disc profile showing the two sections of the phase and the associated phase profile along the cross-section.

The phase profile and the picture illustrated in Figure 4 show a distribution of the refractive index variation inside the GeS<sub>2</sub> material that can be roughly seen as two parts of thickness,  $d_1$  and  $d_2$ . The upper part contributes twice as much as the lower part ( $\varphi_1 = 2\varphi_2$ , which can be deduced from the cross-section phase profile shown in the inset of Figure 4), where  $\varphi_1$  and  $\varphi_2$ , respectively, represent the phase variations in the first part and the second part of the material. Therefore, the total phase variation is  $\varphi = \varphi_1 + \varphi_2 = \frac{3}{2}\varphi_1$ . Thus, for a disc written in a single pass at high energy, we obtain two index variation sections along the z-axis, with a total thickness  $d_1 + d_2 = 80 \mu\text{m}$ :

$$\varphi = \varphi_1 + \varphi_2 = \frac{3}{2}\varphi_1 = \frac{3\pi}{\lambda} d_1 \Delta n_1 \tag{4}$$

with  $d_1 = d_2 = 40 \mu\text{m}$  (estimated from phase profile, see inset of Figure 4). Consequently, with a total phase variation of  $\varphi = 37.8 \text{ rad}$  inside the GeS<sub>2</sub> material (Figure 2), we obtained:

$$\Delta n_1 = \frac{\lambda \varphi}{3\pi d_1} \sim 0.0551 \tag{5}$$

The results presented in Figure 4 confirm the good photosensitivity (i.e.,  $\Delta n$  at “saturation”) of chalcogenide glasses to fs-laser writing. Indeed, refractive index changes

$\Delta n$  up to  $5.5 \times 10^{-2}$  in GeS<sub>2</sub> were successfully implemented. In contrast, the two heavy oxide glasses studied achieved quite large index variations for their class and in particular  $2.08 \times 10^{-2}$  in the Corning 9754 glass and  $6.8 \times 10^{-3}$  in the SF10 glass.

**Implementation of a GRIN lens phase profile using FLDW:** We are now well aware of the phase variation implemented in these materials as a function of laser energy (see Figure 2), and we can now fabricate optical components embedded in the substrate by the fs-laser writing method.

Two types of gradients, described in Figure 5, are possible in order to create the phase profile of a lens by the FLDW technique. We will call the first type a thickness gradient. For this thickness gradient, only one value of refractive index variation is chosen. The phase variation is then created by the superposition of layers of the uniform index but different diameters. It is therefore a classical lens of constant refractive index  $n_1$  immersed in a material of constant index  $n_0$ :  $n_1 = n_0 + \Delta n$ . The second type of gradient is the refractive index gradient. Here, the thickness of the texturing is constant, and it is the refractive index that varies spatially. The index modified by the laser power variation during the writing process is then defined by  $n(r) = n_0 + \Delta n(r)$ . The phase profiles of these two types of gradients are identical but are fabricated in different ways. It will be simpler to manufacture a thickness gradient lens in that only a specific value of index variation is required. It is therefore sufficient to know the laser energy required for a single-phase variation. However, many layers are needed to manufacture a gradient thickness lens, while only one layer may be sufficient for a gradient index lens. The gradient index lens will therefore be written more quickly. For example, Figure 6 shows a 100  $\mu\text{m}$  diameter gradient index lens written on eight layers. The lens was written at a scanning speed of 1 mm/s (corresponding to about 120 pulses/ $\mu\text{m}$ ), and we can see after removing the background in the phase map that the obtained phase profile is equivalent to the designed one.

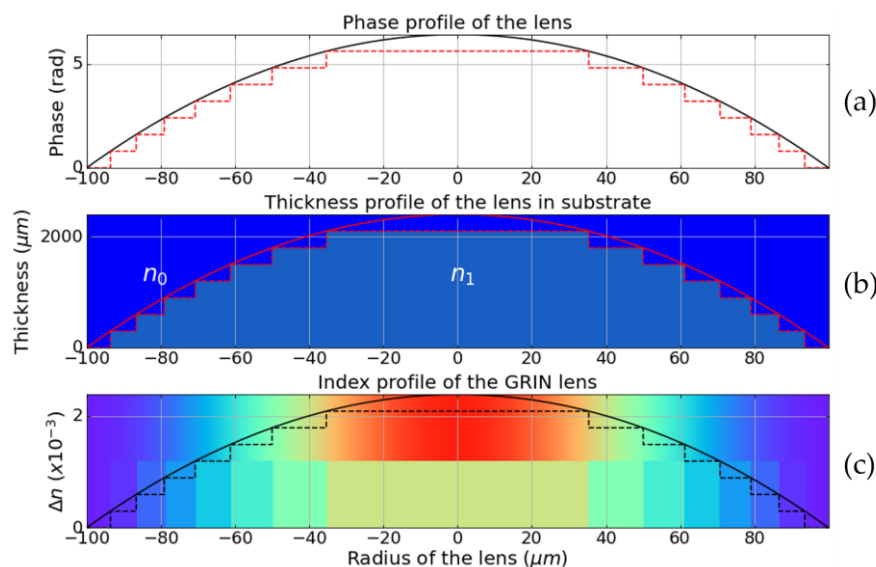


**Figure 5.** (a) GRIN lens phase profile. In black, the continuous phase profile, and in red, the discrete phase profile. (b) Thickness profile of a gradient thickness lens and its discretization corresponding to the phase profile presented in (a). (c) Refractive index profile of a gradient index lens and its discretization corresponding to the phase profile presented in (a). The color variation represents the radial refractive index variation.

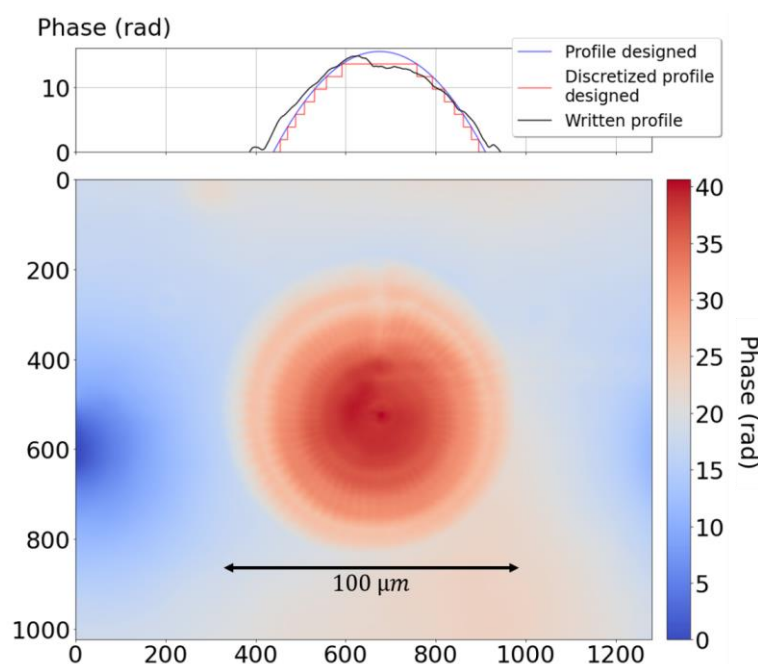


**Figure 6.** Quantitative phase map of a gradient index lens written in GeS<sub>2</sub> glass sample at 1 mm/s scanning speed. Top: plot of the designed profile and the imprinted profile after background subtraction. Laser parameters: 1030 nm, 800 fs, 100 kHz, 0.6 NA.

#### 4. Conclusions

In this paper, we have studied the photosensitivity of one chalcogenide and two commercial heavy oxide glasses to a femtosecond laser direct writing. We have shown the importance of this technique for writing strong refractive index or phase variations at high speed (up to 25 mm/s): up to  $6.8 \times 10^{-3}$  in the SF10,  $2.16 \times 10^{-2}$  in the 9754 and  $5.52 \times 10^{-2}$  in the GeS<sub>2</sub> based chalcogenide. GeS<sub>2</sub> and Corning 9754 are particularly interesting, since they have a good potential to create optical components operating in the mid-infrared. We have obtained a good agreement between the profile of a gradient index lens written by the fs-laser in GeS<sub>2</sub> and the expected one. The femtosecond laser direct writing technique is flexible, so we can plan to create aspherical or even freeform gradient index or complex 3D geometric phase optics, which will improve conventional optical systems. This opens the door to developing a range of efficient and compact components for infrared imaging systems and more generally 3D optics and micro-optics for IR applications.

**Author Contributions:** Conceptualization, M.L.; Investigation, P.D.; Methodology, M.L.; Project administration, G.D., M.L. and B.P.; Resources, L.C. and C.H.; Supervision, G.D., F.D.L.B. and M.L.; Validation, G.D. and M.L.; Writing—original draft, P.D.; Writing—review & editing, P.D., L.C., G.D., F.D.L.B., C.H. and M.L. All authors have read and agreed to the published version of the manuscript.

**Funding:** Agence Nationale de la Recherche (ANR-18-CE08-0004-01); FLAG-IR Project; Research supported by the Ministère des armées—Agence de l’innovation de défense (AID).

**Institutional Review Board Statement:** Not applicable.

**Informed Consent Statement:** Not applicable.

**Conflicts of Interest:** The authors declare no conflict of interest.

## References

1. Davis, K.M.; Miura, K.; Sugimoto, N.; Hirao, K. Writing Waveguides in Glass with a Femtosecond Laser. *Opt. Lett.* **1996**, *21*, 1729. <https://doi.org/10.1364/OL.21.001729>.
2. Fan, C.; Poumellec, B.; Lancry, M.; He, X.; Zeng, H.; Erraji-Chahid, A.; Liu, Q.; Chen, G. Three-Dimensional Photoprecipitation of Oriented LiNbO<sub>3</sub>-like Crystals in Silica-Based Glass with Femtosecond Laser Irradiation. *Opt. Lett.* **2012**, *37*, 2955. <https://doi.org/10.1364/OL.37.002955>.
3. Unal, A.A.; Stalmashonak, A.; Seifert, G.; Graener, H. Ultrafast Dynamics of Silver Nanoparticle Shape Transformation Studied by Femtosecond Pulse-Pair Irradiation. *Phys. Rev. B* **2009**, *79*, 115411. <https://doi.org/10.1103/PhysRevB.79.115411>.
4. Shimotsuma, Y.; Kazansky, P.G.; Qiu, J.; Hirao, K. Self-Organized Nanogratings in Glass Irradiated by Ultrashort Light Pulses. *Phys. Rev. Lett.* **2003**, *91*, 247405. <https://doi.org/10.1103/PhysRevLett.91.247405>.
5. Arriola, A.; Gross, S.; Ams, M.; Gretzinger, T.; Le Coq, D.; Wang, R.P.; Eborndorff-Heidepriem, H.; Sanghera, J.; Bayya, S.; Shaw, L.B.; et al. Mid-Infrared Astrophotonics: Study of Ultrafast Laser Induced Index Change in Compatible Materials. *Opt. Mater. Express* **2017**, *7*, 698. <https://doi.org/10.1364/OME.7.000698>.
6. Gandara-Montano, G.A.; Ivansky, A.; Savage, D.E.; Ellis, J.D.; Knox, W.H. Femtosecond Laser Writing of Freeform Gradient Index Microlenses in Hydrogel-Based Contact Lenses. *Opt. Mater. Express* **2015**, *5*, 2257. <https://doi.org/10.1364/OME.5.002257>.
7. Roux, F.S. Geometric Phase Lens. *J. Opt. Soc. Am. A* **2006**, *23*, 476. <https://doi.org/10.1364/JOSAA.23.000476>.
8. Beresna, M.; Gecevičius, M.; Kazansky, P.G. Ultrafast Laser Direct Writing and Nanostructuring in Transparent Materials. *Adv. Opt. Photonics* **2014**, *6*, 293–339.
9. Eaton, S.M.; Ng, M.L.; Osellame, R.; Herman, P.R. High Refractive Index Contrast in Fused Silica Waveguides by Tightly Focused, High-Repetition Rate Femtosecond Laser. *J. Non-Cryst. Solids* **2011**, *357*, 2387–2391. <https://doi.org/10.1016/j.jnoncrysol.2010.11.082>.
10. Drevinskas, R.; Beresna, M.; Gecevičius, M.; Khenkin, M.; Kazanskii, A.G.; Matulaitienė, I.; Niaura, G.; Konkov, O.I.; Terukov, E.I.; Svirko, Y.P.; et al. Giant Birefringence and Dichroism Induced by Ultrafast Laser Pulses in Hydrogenated Amorphous Silicon. *Appl. Phys. Lett.* **2015**, *106*, 171106. <https://doi.org/10.1063/1.4919538>.
11. Bérubé, J.P.; Messaddeq, S.H.; Bernier, M.; Skripachev, I.; Messaddeq, Y.; Vallée, R. Tailoring the Refractive Index of Ge-S Based Glass for 3D Embedded Waveguides Operating in the Mid-IR Region. *Opt. Express* **2014**, *22*, 26103. <https://doi.org/10.1364/OE.22.026103>.
12. Gross, S.; Jovanovic, N.; Sharp, A.; Ireland, M.; Lawrence, J.; Withford, M.J. Low Loss Mid-Infrared ZBLAN Waveguides for Future Astronomical Applications. *Opt. Express* **2015**, *23*, 7946. <https://doi.org/10.1364/OE.23.007946>.
13. Bérubé, J.-P.; Le Camus, A.; Messaddeq, S.H.; Petit, Y.; Messaddeq, Y.; Canioni, L.; Vallée, R. Femtosecond Laser Direct Inscription of Mid-IR Transmitting Waveguides in BGG Glasses. *Opt. Mater. Express* **2017**, *7*, 3124. <https://doi.org/10.1364/OME.7.003124>.
14. Zhou, W.; Li, R.; Li, M.; Tao, P.; Wang, X.; Dai, S.; Song, B.; Zhang, W.; Lin, C.; Shen, X.; et al. Fabrication of Microlens Array on Chalcogenide Glass by Wet Etching-Assisted Femtosecond Laser Direct Writing. *Ceram. Int.* **2022**, *48*, 18983–18988. <https://doi.org/10.1016/j.ceramint.2022.03.181>.
15. Lippman, D.H.; Kochan, N.S.; Yang, T.; Schmidt, G.R.; Bentley, J.L.; Moore, D.T. Freeform Gradient-Index Media: A New Frontier in Freeform Optics. *Opt. Express* **2021**, *29*, 36997. <https://doi.org/10.1364/OE.443427>.
16. Petit, L.; Carlie, N.; Anderson, T.; Jiyeon Choi; Richardson, M.; Richardson, K.C. Progress on the Photoresponse of Chalcogenide Glasses and Films to Near-Infrared Femtosecond Laser Irradiation: A Review. *IEEE J. Select. Top. Quantum Electron.* **2008**, *14*, 1323–1334. <https://doi.org/10.1109/JSTQE.2008.922898>.
17. Glezer, E.N.; Milosavljevic, M.; Huang, L.; Finlay, R.J.; Her, T.-H.; Callan, J.P.; Mazur, E. Three-Dimensional Optical Storage inside Transparent Materials. *Opt. Lett.* **1996**, *21*, 2023. <https://doi.org/10.1364/OL.21.002023>.
18. Yao, H.; Zaiter, R.; Cavillon, M.; Sapaly, B.; Calzavara, F.; Deluillier, P.; Cardinal, T.; Dai, Y.; Poumellec, B.; Lancry, M. Photosensitivity of Barium Germano-Gallate Glasses under Femtosecond Laser Direct Writing for Mid-IR Applications. *Ceram. Int.* **2021**, *47*, 34235–34241. <https://doi.org/10.1016/j.ceramint.2021.08.333>.
19. Zhang, F.; Cerkauskaite, A.; Drevinskas, R.; Kazansky, P.G.; Qiu, J. Microengineering of Optical Properties of GeO<sub>2</sub> Glass by Ultrafast Laser Nanostructuring. *Adv. Opt. Mater.* **2017**, *5*, 1700342. <https://doi.org/10.1002/adom.201700342>.
20. Masselin, P.; Le Coq, D.; Cuisset, A.; Bychkov, E. Spatially Resolved Raman Analysis of Laser Induced Refractive Index Variation in Chalcogenide Glass. *Opt. Mater. Express* **2012**, *2*, 1768. <https://doi.org/10.1364/OME.2.001768>.
21. Schaffer, C.B. *Interaction of Femtosecond Laser Pulses with Transparent Materials*; Harvard University: Cambridge, MA, USA, 2001.
22. Lenzner, M.; Krüger, J.; Kautek, W.; Krausz, F. Incubation of Laser Ablation in Fused Silica with 5-Fs Pulses. *Appl. Phys. A Mater. Sci. Processing* **1999**, *69*, 465–466. <https://doi.org/10.1007/s003390051034>.
23. Ashkenasi, D.; Lorenz, M.; Stoian, R.; Rosenfeld, A. Surface Damage Threshold and Structuring of Dielectrics Using Femtosecond Laser Pulses: The Role of Incubation. *Appl. Surf. Sci.* **1999**, *150*, 101–106. [https://doi.org/10.1016/S0169-4332\(99\)00228-7](https://doi.org/10.1016/S0169-4332(99)00228-7).
24. Stoian, R. Investigations of the Dynamics of Material Removal in Ultrashort Pulsed Laser Ablation of Dielectrics. Ph.D. Thesis, Freien Universität Berlin: Berlin, Germany, 2000.
25. Muzi, E.; Cavillon, M.; Lancry, M.; Brisset, F.; Que, R.; Pugliese, D.; Janner, D.; Poumellec, B. Towards a Rationalization of Ultrafast Laser-Induced Crystallization in Lithium Niobium Borosilicate Glasses: The Key Role of the Scanning Speed. *Crystals* **2021**, *11*, 290. <https://doi.org/10.3390/cryst11030290>.

26. Zuo, C.; Li, J.; Sun, J.; Fan, Y.; Zhang, J.; Lu, L.; Zhang, R.; Wang, B.; Huang, L.; Chen, Q. Transport of Intensity Equation: A Tutorial. *Opt. Lasers Eng.* **2020**, *135*, 106187. <https://doi.org/10.1016/j.optlaseng.2020.106187>.
27. McMillen, B.; Zhang, B.; Chen, K.P.; Benayas, A.; Jaque, D. Ultrafast Laser Fabrication of Low-Loss Waveguides in Chalcogenide Glass with 0.65 DB/cm Loss. *Opt. Lett.* **2012**, *37*, 3. <https://doi.org/10.1364/OL.37.001418>.
28. Jain, A.; Hautier, G.; Ong, S.P.; Moore, C.J.; Fischer, C.C.; Persson, K.A.; Ceder, G. Formation Enthalpies by Mixing GGA and GGA + U Calculations. *Phys. Rev. B* **2011**, *84*, 045115. <https://doi.org/10.1103/PhysRevB.84.045115>.
29. Stoian, R. Volume Photoinscription of Glasses: Three-Dimensional Micro- and Nanostructuring with Ultrashort Laser Pulses. *Appl. Phys. A* **2020**, *126*, 438. <https://doi.org/10.1007/s00339-020-03516-3>.
30. Gross, S.; Lancaster, D.G.; Ebendorff-Heidepriem, H.; Monro, T.M.; Fuerbach, A.; Withford, M.J. Femtosecond Laser Induced Structural Changes in Fluorozirconate Glass. *Opt. Mater. Express* **2013**, *3*, 574. <https://doi.org/10.1364/OME.3.000574>.
31. Messaddeq, S.H.; Bérubé, J.P.; Bernier, M.; Skripachev, I.; Vallée, R.; Messaddeq, Y. Study of the Photosensitivity of GeS Binary Glasses to 800nm Femtosecond Pulses. *Opt. Express* **2012**, *20*, 2824. <https://doi.org/10.1364/OE.20.002824>.